Catalysts **2013**, *3*, 444-454; doi:10.3390/catal3020444

OPEN ACCESS

catalysts

ISSN 2073-4344

www.mdpi.com/journal/catalysts

Article

Manganese Oxide-Surface Modified Titanium(IV) Dioxide as Environmental Catalyst

Qiliang Jin, Hiroshi Arimoto, Musashi Fujishima and Hiroaki Tada *

Department of Applied Chemistry, School of Science and Engineering, Kinki University, 3-4-1, Kowakae, Higashi-Osaka, Osaka 577-8502, Japan; E-Mails: ql_jin@hotmail.com (Q.J.); earnest-tyk.n-twilight@ezweb.ne.jp (H.A.); mfujishima@apch.kindai.ac.jp (M.F.)

* Author to whom correspondence should be addressed; E-Mail: h-tada@apch.kidai.ac.jp; Tel.: +81-6-6721-2332; Fax: +81-6-6727-2024.

Received: 23 December 2012; in revised form: 10 April 2013 / Accepted: 12 April 2013 / Published: 23 April 2013

Abstract: The purpose of this study is to present an "environmental catalyst" possessing both thermocatalytic activity and visible-light activity for the decomposition of organic pollutants. Molecule-sized MnO_x clusters are highly dispersed on the surface of TiO_2 (anatase/rutile = 4/1 *w*/*w*, P-25, Degussa) by the chemisorption-calcination cycle technique using $Mn(acac)_3$ complex as a precursor (MnO_x/TiO_2). The thermo- and photo-catalytic activities of MnO_x/TiO_2 were studied for the degradation of 2-naphthol used as a model water pollutant. In contrast to the FeO_x/TiO_2 system, MnO_x/TiO_2 exhibits high thermocatalytic activity exceeding those of bulk β-β-MnO_2 and Mn_2O_3. Also, visible-light activity is induced by the surface modification of TiO_2 with MnO_x clusters, whereas its UV-light activity decreases.

Keywords: titanium dioxide; manganese oxides; surface modification; thermocatalytic activity; photocatalytic activity; environmental catalyst

1. Introduction

At present the development of catalysts effectively purifying polluted air and water is highly desired for the conservation of human health. Among the "environmental catalysts", TiO_2 photocatalyst is the most promising one, due to the strong oxidation ability to completely mineralize organic pollutants, long-term durability, and abundance in nature [1,2]. A serious drawback of

photocatalysts in their practical use is that they do not work in the dark, which narrows their applications. On the other hand, manganese oxides such as MnO_2 and Mn_2O_3 [3–5] and manganese-cerium [6] mixed oxides are known to exhibit thermocatalytic activity for the decomposition of organic pollutants, although the activity at ambient temperature falls short of the TiO_2 photocatalytic activity. Previously, the coupling system of TiO_2 and β-MnO_2 nanoparticle was prepared by a photodeposition technique (MnO_2 NP/TiO_2) [7]. This heterostructured system shows a simple additive effect of MnO_2 and TiO_2, *i.e.*, the degradation of organics due to the thermocatalytic activity of MnO_2 is enhanced by the UV-light irradiation because of the TiO_2 photocataltyic activity. The key to increasing the thermocatalytic activity is the high dispersion of manganese oxide (MnO_x) clusters on the TiO_2 surface. We have developed the chemisorption-calcination cycle (CCC) technique for forming extremely small metal oxide clusters on metal oxide supports such as TiO_2 [8]. This process consists of metal complex chemisorption on the support and subsequent thermal oxidation of organic ligands enables the formation of molecule-sized metal oxide clusters on the TiO_2 surface in a highly dispersed state. Meanwhile, the visible-light activation of TiO_2 is an important subject in terms of the effective utilization of sunlight, because only 3–4% of the solar energy is harnessed by TiO_2 with a large band gap (3–3.2 eV) [9,10]. Recently, it has been revealed by means of spectroscopic experiments and first principles density functional theory simulations, that the band structure of TiO_2 can effectively be tuned by its surface modification with very small metal oxide clusters such as FeO_x and NiO [11–15]. As a result, high levels of visible-light activities are endowed with TiO_2, and, concomitantly, UV-light activities remarkably increase. The photocatalytic activity of the metal oxide cluster-surface modified TiO_2 (MO/TiO_2) strongly depends on the kinds of metal oxides used [16] and the crystal form of TiO_2 [17]. The photocatalytic activity of Mn-doped TiO_2 has recently been demonstrated to work under visible-light illumination for removing gaseous acetaldehyde [18]. Consequently, MnO_x/TiO_2 prepared by the CCC technique can be expected to perform as an "environmental catalyst" working in the dark and under visible-light illumination.

Here we report the preparation of MnO_x/TiO_2 (P-25, Degussa) by the CCC technique, and the thermo-and photo-catalytic activities for the degradations of model organic pollutants.

2. Results and Discussion

2.1. Control of the Mn-Loading Amount

The photocatalytic activity of MO/TiO_2 is sensitive to the loading amount of metal oxide clusters [11–14]. A feature of the CCC technique is precise control of the loading amount of metal oxides. Figure 1A shows the relation between the Mn-loading amount after heating Mn complex-adsorbed P-25 at 773 K in air (Γ/ions nm^{-2}) and the initial concentration of $Mn(acac)_3$ ($[Mn(acac)_3]_0$). The Γ value steeply increases at $[Mn(acac)_3]_0 < 2$ mmol dm^{-3} to reach ~0.75 ions nm^{-2} at $[Mn(acac)_3]_0 = 8$ mmol dm^{-3}. Figure 1B shows plots of Γ *versus* the number of the chemisorption-calcination cycle (n) at $[Mn(acac)_3]_0 = 8$ mmol dm^{-3}. The Γ value further increases almost in proportional to n. In this manner, the Mn-loading amount can be controlled by the $Mn(acac)_3$ concentration at $\Gamma < 1$ and by the n value at $\Gamma > 1$.

Figure 1. (**A**) Plots of the Mn-loading amount (Γ/ions nm^{-2}) *versus* initial concentration of $Mn(acac)_3$ ($[Mn(acac)_3]_0$); (**B**) Plots of Γ *versus* chemisorption-calcination cycle number (n) at $[Mn(acac)_3]_0 = 8$ mmol dm^{-3}.

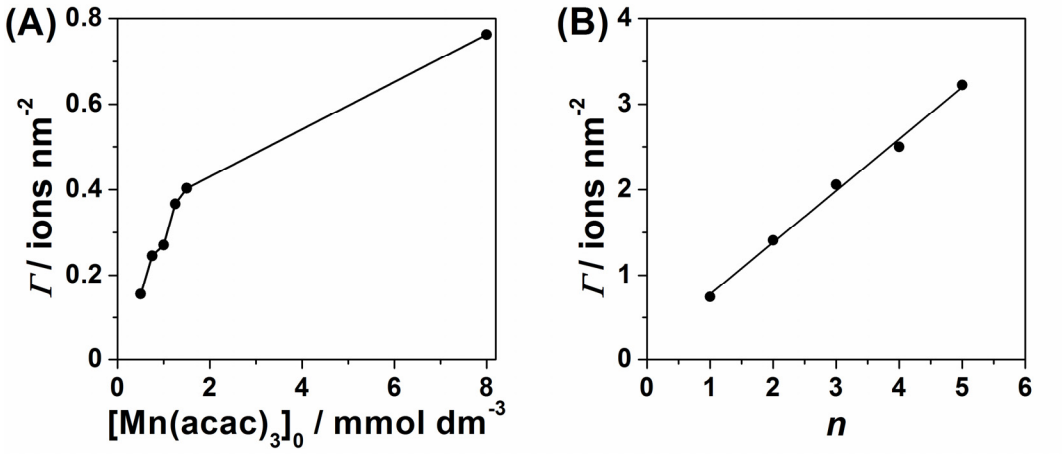

2.2. Characterization Results

Transmission electron micrographs of the samples with varying Γ are shown in Figure 2. No particulate deposits are observed on the P-25 surface even for the sample with $\Gamma \approx 3$. This fact indicates that molecular scale Mn oxide species (MnO_x) are formed on the P-25 surface by the CCC technique in a similar manner as the FeO_x/TiO_2 [11–13] and SnO_2/TiO_2 [17,19] systems, whereas NiO deposits as cluters smaller than ~2 nm [14].

The optical properties are of primary importance for the photocatalytic activity. Figure 3 shows UV-visible absorption spectra of MnO_x/P-25 samples with varying Γ. Pristine P-25 has hardly any absorption at $\lambda > 400$ nm. The surface modification of P-25 with MnO_x clusters causes new absorption in the whole visible region like the Mn-doped TiO_2 system [18]. Also, the absorption intensity in the UV region decreases with increasing λ. For comparison, the spectra for bulk β-MnO_2 and Mn_2O_3 physically mixed with P-25 are also shown. They possess intense featureless absorption in the whole visible region, of which intensity is almost independent of λ. In this manner, the surface modification of P-25 with MnO_x clusters by the CCC technique causes unique absorption in the visible region (*vide infra*).

Figure 2. TEMs of MnO_x/TiO_2 samples with varying Mn-loading amount (Γ/ions nm^{-2}): (**A**) P-25; (**B**) $\Gamma = 0.16$; (**C**) $\Gamma = 0.76$; (**D**) $\Gamma = 3.0$.

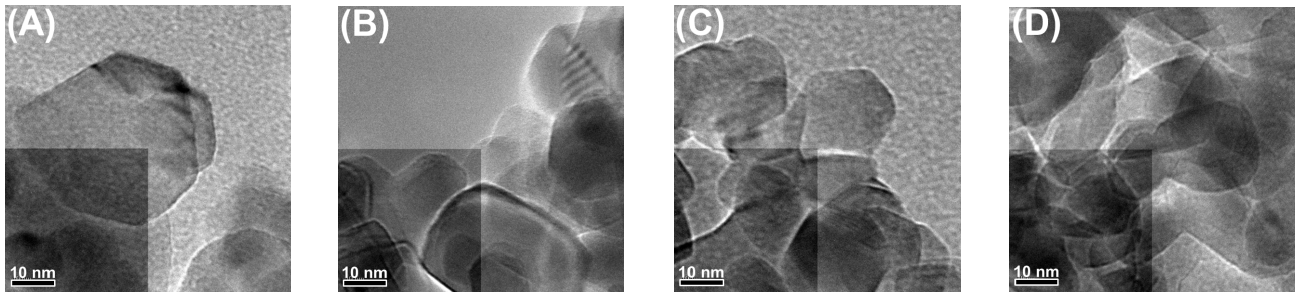

Figure 3. UV-visible absorption spectra of MnO_x/P-25 samples with varying Mn-loading amounts (Γ/ions nm^{-2}).

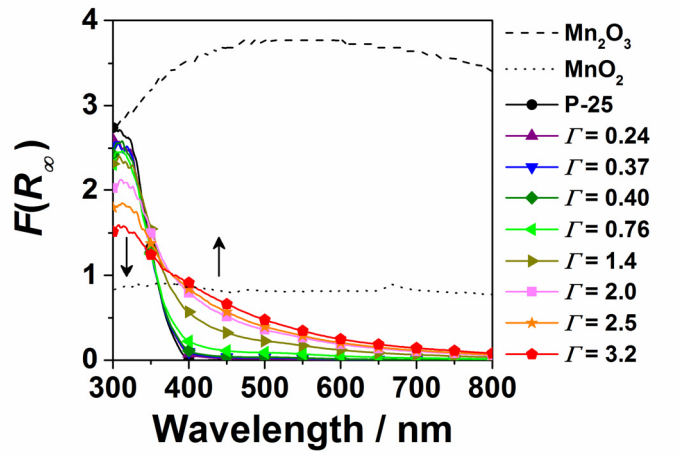

To gain the information regarding the oxidation state of Mn ions in the MnO_x clusters, X-ray photolectron spectroscopic (XPS) measurements were performed. Figure 4A shows Mn2p-XPS spectra of MnO_x/P-25 samples with varying Γ. In the spectra of authentic manganese oxides (β-MnO_2, Mn_2O_3, and MnO), Mn 2p3/2 and Mn 2p1/2 signals are observed in the regions of 640.8-642.5 eV and 652.8–653.6 eV, respectively. In the spectra for MnO_x(Γ > 1.1)/P-25, the E_B(Mn2 p3/2) and E_B(Mn 2p1/2) are located at 641.5 eV and 653.2 eV (spin-orbit splitting of 11.7 eV), respectively, which are close to the values for Mn_2O_3 [20]. The shift of the E_B(Mn 2p3/2) towards lower energy for the sample with Γ = 0.4 suggests the co-existence of Mn ions with lower oxidation states. Previously, Mn species highly dispersed on SiO_2 by means of solvated metal atom dispersed method were reported to exist as MnO and Mn_2O_3 [20]. Thus, the main oxidation state of Mn in the MnO_x clusters is +3, and lower oxidation states mixes at Γ < 0.4.

Figure 4. Mn2p-XPS (**A**) and valence band-XPS; (**B**) spectra of MnO_x/P-25 samples with varying Mn-loading amounts (Γ/ions nm^{-2}).

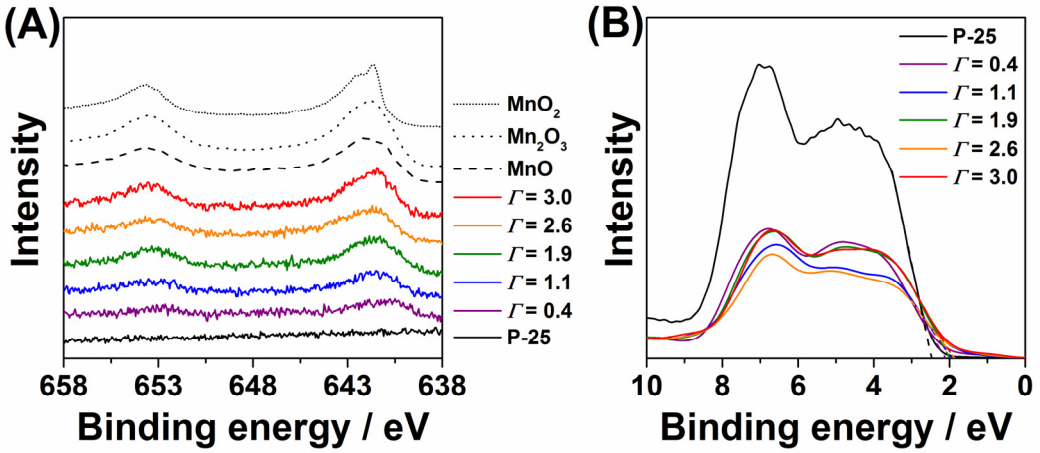

Further, to study the cause of the visible absorption induced by the MnO_x surface modification, valence band (VB)-XPS was measured. Figure 4B shows the VB-XPS spectra of MnO_x/P-25 samples with varying Γ. The emission from the O2p–VB extends from 2 to 9 eV. Closer inspection indicates

that the top of VB slightly rises with an increase in $\tilde{\Gamma}$ The magnitude of the change in the top of VB reaches *ca*. 0.5 eV at $\Gamma \approx 1$. Mixing between the surface Mn 3d levels and O2p is considered as yielding a surface d-band dispersing around the energy level to overlap with the VB(TiO_2) [16]. Consequently, bandgap narrowing is induced by the surface modification of TiO_2 with MnO_x clusters in the same manner as the FeO_x- [11–13] and NiO- [14] surface modified systems. Thus, the absorption below ~500 nm might be attributed to the transition from the surface d-band to the CB(TiO_2) or the surface-to-bulk interfacial electron transfer.

Electrochemical measurements were carried out to examine the redox property of MnO_x/P-25. Figure 5 shows cyclic voltammograms (CV) for mesoporous P-25 film-coated FTO electrodes with MnO_x surface modification. In the CV curves without O_2, a pair of redox currents due to the redox reaction of manganese ions is observed. This redox reaction can be formally written by Equation (1).

$$Mn^{m+}(MnO_x) + e^- \Leftrightarrow Mn^{(m-1)+}(MnO_x) \quad (1)$$

$$Mn^{(m-1)+}(MnO_x) + 1/4O_2(aq) \rightarrow Mn^{m+}(MnO_{x+0.5}) \quad (2)$$

Interestingly, the currents remarkably decrease in the presence of O_2. This finding could be explained by assuming the smooth non-electrochemcial oxidation of the reduced manganese oxide by O_2, dissolved in the reaction solution. Also, the MnO_x-surface modification did not enhance the O_2 reduction unlike the FeO_x- and NiO-surface modification systems [11–14].

Figure 5. Cyclic voltammograms (CV) curves for mesoporous P-25 film-coated fluorine-doped SnO_2 (FTO) electrodes with MnO_x surface modification in the absence and presence of O_2.

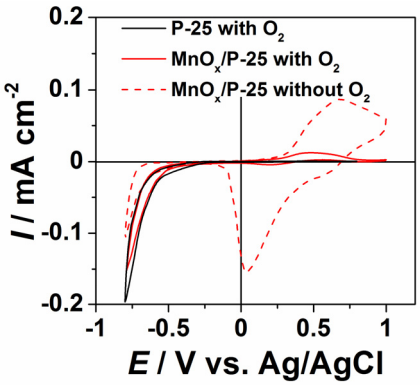

2.3. Thermocatalytic Activity

As a test reaction, 2-naphthol degradation was carried out at 323 K in the dark. Figure 6A shows plots of ln (C_0/C) *versus* reaction time (t_d) for the MnO_x/P-25-catalyzed 2-naphthol degradation: C_0 and C denote the 2-naphthol concentrations at $t_d = 0$ and $t_d = t$, repectively. In every system, the reaction follows the frst-order kinetic behavior, within the precision of the experiments. The rate coefficient of the reaction increased with increasing temperature. Increasing temperature generally suppresses the adsorption process with negative entropy change, and thus, the decrease in the 2-naphthol concentration mainly results, not from the adsorption, but from the degradation. From the

Arrhenius plot, the activation energy was determined to be 32.5 ± 4.0 kJ mol^{-1}. The turnover number of the 2-naphthol degradation reaches 10 at reaction time = 2 h. Under deaerated conditions, the 2-naphthol degradation took place; however, the turnover number did not exceed unity. Clearly, this reaction proceeds catalytically under aerated conditions.

The relation between the first-order rate coefficient (k_d) and Γ is shown in Figure 6B. While P-25 is almost inactive, the k_d value increases with an increase in Γ. This fact indicates that the surface MnO_x clusters act as catalytically active centers. The activity of MnO_x(Γ = 3.2)/P-25 (k_d = 0.30) is greater than those of β-MnO_2 (k_d = 0.10) and Mn_2O_3 (k_d = 0.25) in spite that the Mn amount in the reaction system is only ~1/50. This high level of thermocatalytic activity of MnO_x/P-25 can be attributed to the extremely high dispersion state of MnO_x species on the surface of TiO_2 with a large surface area. This catalytic reaction may be explained by the Mars-van Krevelen mechanism, in which the manganese oxide clusters oxidize hydrocarbons (Equation (1)), and O_2 in the solution oxidizes back the reduced manganese oxide clusters (Equation (2)) [3].

Figure 6. (**A**) Plots of ln (C_0/C) *versus* reaction time (t_d) for the 2-naphthol degradation at 323 K in the dark: C_0 and C denote the 2-naphthol concentrations at t_d = 0 and t_d = t, repectively; (**B**) Plots of rate coefficient (k_d) *versus* Mn-loading amount (Γ/ions nm^{-2}).

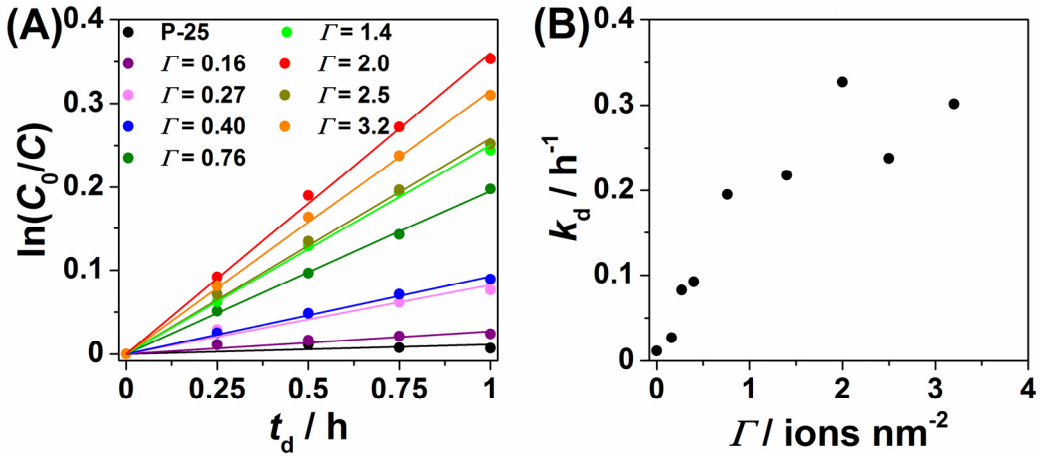

Figure 7. Plots of ln (C_0/C) *versus* irradiation time (t) for the 2-naphthol degradation under visible-light irradiation (**A**) and UV-light irradiation; (**B**) C_0 and C denote the 2-naphthol concentrations at t_d = 0 and t_d = t, repectively.

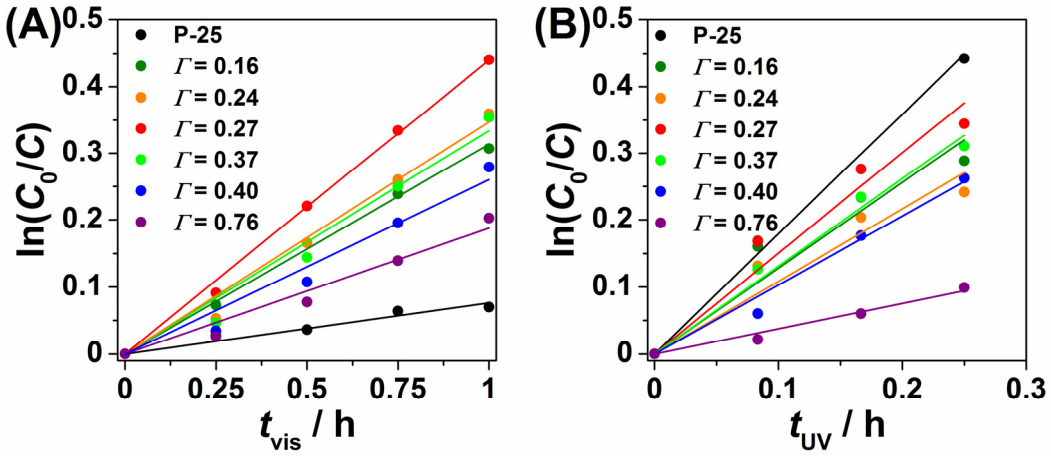

2.4. Photocataltyic Activity

Photocatalytic activities of MnO_x/P-25 samples were examined under UV- and visible-light irradiation at 298 K. As shown in Figure 6B, the thermocatalytic activity is fairly low at $\Gamma < 0.4$, and it is negligibly small as compared with the photocatalytic activity at 298 K. Figure 7 shows plots of ln (C_0/C) *versus* irradiation time (t_p) for the 2-naphthol degradation under visible-light irradiation (A) and UV-light irradiation (B). In both the cases, the 2-naphthol degradation obeys the first-order kinetic behavior, within the precision of the experiments.

Figure 8A shows the first-order rate constant for the 2-naphthol degradation under visible-light irradiation (k_{vis}/h^{-1}) as a function of Γ. Whereas the activity of pristine P-25 is low, MnO_x/P-25 samples show much higher levels of visible-light activity with a maximum of 0.43 h^{-1} at $\Gamma = 0.27$.

Figure 8. First-order rate coefficient for the 2-naphthol degradation under visible- (**A**, k_{vis}) and UV-light irradiation (**B**, k_{UV}) as a function of Mn-loading amount (Γ/ions nm^{-2}).

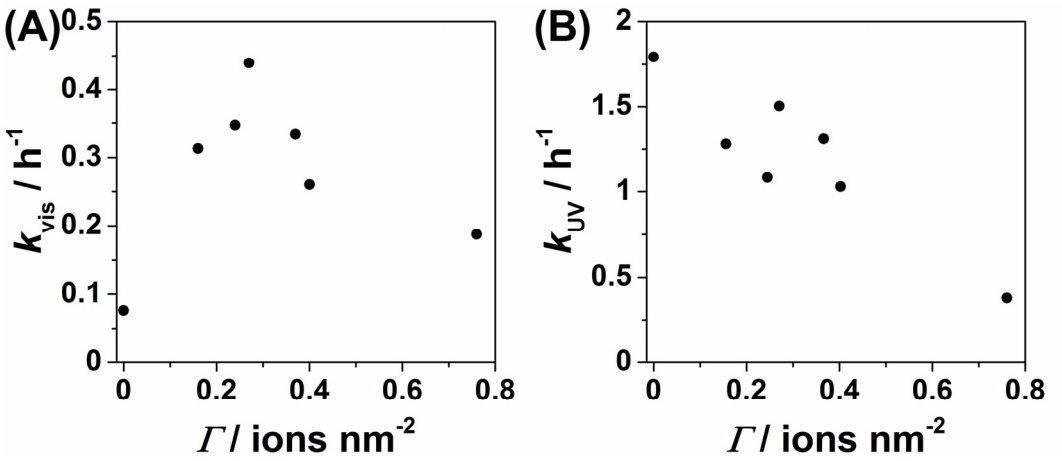

Table 1. Photocatalytic activities of metal oxide-surface modified TiO_2 (P-25) for the 2-naphthol degradation [a].

Surface modifier	k_{UV}/h^{-1} [b]	k_{vis}/h^{-1} [c]
none	1.8 ± 0.23	0.09 ± 0.015
MnO_x	1.5 (0.27)	0.43± 0.011 (0.27)
FeO_x	6.9 ± 0.8 (0.54)	0.69 ± 0.02 (0.49)
NiO	5.0 ± 1.0 (0.47)	1.3 ± 0.1 (0.32)
CuO	6.1 (0.025)	0.47 (0.50)
SnO_2	1.9 (0.025)	0.08 (0.032)

[a] The values in the parentheses show the optimum metal loading amount (ions nm^{-2}); [b] First-order rate constant for the 2-naphthol oxidation under UV-light irradiation ($330 < \lambda < 400$ nm, $I_{320–400\ nm} = 0.5$ mW cm^{-2}); [c] First-order rate constant for the 2-naphthol oxidation under visible-light irradiation ($\lambda > 400$ nm, $I_{420–485\ nm} = 1.0$ mW cm^{-2}).

Table 1 compares the k_{vis} values for various metal oxide cluster-surface modified P-25 evaluated under the same conditions. The maximum visible-light activity of several metal oxide-surface modified P-25 is on the order of NiO > FeO_x > CuO ≈ MnO_x > SnO_2 ≈ none under the same conditions.

The visible-light activity can be induced by the electronic transition from the surface d-band to the conduction band (CB) of TiO_2. Recently, we have clarified that the TiO_2-photocatalyzed degradation of 2-naphthol proceeds via the direct hole oxidation by density functional theory calculations [21]. Also in this system, 2-naphthol can be oxidized by the holes generated in the surface d-band, while the electrons in the CB(TiO_2) reduce O_2. As a result of the increase in Γ, the visible-light absorption of MnO_x/P-25 increases (Figure 3), while the oxidation ability of the holes lowers with the rise in the top of VB (Figure 4B). The balance between the visible-light absorption intensity and the oxidation power of the holes determines the optimum Γ.

Figure 8B shows the first-order rate constant for the 2-naphthol degradation under UV-light irradiation (k_{UV}/h^{-1}) as a function of Γ. The k_{UV} value significantly decreases with increasing Γ in contrast to the FeO_x/TiO_2 [11,12] and NiO/TiO_2 [13] systems, where a high level of visible-light activity appears concomitantly with the UV-light remarkably increased. The maximum UV-light activity is on the order of FeO_x > CuO > NiO > SnO_2 ~ none > MnO_x under the same conditions (Table 1). The surface MnO_x clusters hardly affect the reduction of O_2 (Figure 5). Thus, the decrease in the UV-light absorption with the surface MnO_x modification can mainly be attributed to the lowering in the UV-light activity.

3. Experimental Section

3.1. Materials

As a standard TiO_2 photocatalyst, Degussa P-25 (anatase/rutile = 4/1 *w*/*w*, specific surface area S_{BET} = 50 $m^2\ g^{-1}$, P-25) were used. Also, β-MnO_2 (S_{BET} = 0.1 $m^2\ g^{-1}$, Kishida Chemical, Osaka, Japan), Mn_2O_3 (S_{BET} = 6.26 $m^2\ g^{-1}$, Kishida Chemical), and MnO (Kishida Chemical) particles were used for comparison.

3.2. Catalyst Preparation

Manganese oxide-surface modified TiO_2 (anatase/rutile = 4/1 *w*/*w*, P-25, Degussa, Düsseldorf, Germany) powders were prepared using manganese (III) acetylacetonate ($Mn(acac)_3$) as a precursor. After TiO_2 particles (2 g) were added to ethanol $Mn(acac)_3$ solutions with different concentrations, they were allowed to stand for 24 h at 298 K in the dark. The resulting samples were washed with ethanol, and dried at room temperature for 24 h in vacuum, and heated in air at 773 K for 1 h. MnO_x/P-25 particles (0.2 g) were added to a mixed solution of water (0.5 mL) and Triton X-100 (0.25 mL). After sufficiently mixing, the resulting paste was coated on fluorine-doped SnO_2 (FTO) electrode, and then heated at 673 K for 1 h.

3.3. Catalyst Characterization

MnO_x/TiO_2 (0.02 g) was dissolved into hot sulfuric acid (98%, 5 mL). The solution was diluted three times in volume with water, and then the Mn concentration was determined by inductively

coupled plasma spectroscopy (ICPS-7500, Shimadzu). The morphologies of MnO_x/TiO_2 powders were observed by transmission electron microscopy (TEM), using a JEM-3010F electron microscope (JEOL, Tokyo, Japan) at an acceleration voltage of 300 kV. UV-visible diffuse reflectance spectra of MnO_x/TiO_2 were recorded on a Hitachi U-4000 spectrophotometer. The spectra were converted to the absorption spectra by using the Kubelka-Munk function. X-ray photoelectron spectroscopic (XPS) measurements were performed using a Kratos Axis Nova X-ray photoelectron spectrometer with a monochromated Al Kα X-ray source (hν = 1486.6 eV) operated at 15 kV and 10 mA. The take-off angle was 90º, and multiplex spectra were obtained for Mn2p, O1s, and Ti2p photopeaks. All the binding energies (EB) were referenced with respect to the C1s at 284.6 eV. Current-potential curves of the MnO_x/ P-25/FTO electrodes were measured in a 0.1 M Na_2ClO_4 electrolyte solution in a regular three-electrode electrochemical cell using a galvanostat/potentiostat (HZ-5000, Hokuto Denko, Tokyo, Japan). Glassy carbon and an Ag/AgCl electrode (TOA-DKK) were used as a counter electrode and a reference electrode, respectively.

3.4. Thermocatalytic Activity Evaluation

P-25 or MnO_x/P-25 particles (0.1 g) was placed in 50 mL of 1.0×10^{-5} mol dm^{-3} 2-naphthol solution (solvent, acetonitrile:water = 1 : 99 *v*/*v*) in a flask , and stirred in the dark at 323 K. Two mL of the solution was sampled every 15 min, and its electronic absorption spectrum was measured using a photospectrometer (Shimadzu, UV-1800, Kyoto, Japan). The concentration of 2-naphthol was determined from the absorption peak at 224 nm ($\varepsilon_{max} = 6.79 \times 10^4$ mol^{-1} dm^3 cm^{-1}).

3.5. Photocataltyic Activity Evaluation

P-25 or MnO_x/P-25 particles (0.1 g) was added to 50 mL of 1.0×10^{-5} mol dm^{-3} 2-naphthol (solvent, acetonitrile : water = 1:99 *v*/*v*) in a borosilicate glass container was irradiated. The reaction cell was irradiated with a Xe lamp (Wacom XRD-501SW) through a band-pass filter (33U, SIGMA KOKI CO., Ltd., Tokyo, Japan) superposed on two pieces of glass plates with fluorine-doped tin oxide film (FTO) transmitting only the 330-400 nm range for the UV-light activity test and a high pass filter (L-42, Toshiba) to cut off UV-light for the visible-light activity test. Two mL of the solution was sampled at given irradiation time, and the 2-napthol concentration was determined from its electronic absorption spectra.

4. Conclusions

We have prepared molecular scale MnO_x cluster-surface modified TiO_2 by the CCC technique (MnO_x/TiO_2) with the loading amount precisely controlled. MnO_x/TiO_2 exhibits a high level of thermocatalytic activity for the degradation of 2-naphthol. The thermocatalytic activity increases with increasing Mn loading amount at <3 ions nm^{-2}. Also, as a result of the surface modification by MnO_x clusters, fairly high visible-light activity is endowed with TiO_2, whereas the UV-light activity decreases. This paper has presented a prototype of a TiO_2-based environmental catalyst working with and without light irradiation.

Acknowledgements

Hiroaki Tada acknowledges supports from the Ministry of Education, Science, Sport, and Culture, Japan through a Grant-in-Aid for Scientific Research (C) No. 24550239, and Nippon Sheet Glass Foundation for Materials Science and Engineering, and by Sumitomo Foundation.

References

1. Fujishima, A.; Zhang, X.; Tryk, D.A. TiO_2 photocatalysis and related surface phenomena. *Surf. Sci. Rep*. **2008**, *63*, 515–582.
2. Hashimoto, K.; Irie, H.; Fujishima, A. TiO_2 photocatalysis: A historical overview and future prospects. *Jpn. J. Appl. Phys*. **2005**, *44*, 8269–8285.
3. Sinha, A.K.; Suzuki, K.; Takahara, M.; Azuma, H.; Nonaka, T.; Fukumoto, K. Mesostructured manganese oxide/gold nanoparticle composites for extensive air purification. *Angew. Chem. Int. Ed.* **2007**, *46*, 2891–2894.
4. Chen, H.; He, J.; Zhang, C.; He, H. Self-assembly of novel mesoporous manganese oxide nanostructures and their application in oxidative decomposition of formaldehyde. *J. Phys. Chem. C* **2007**, *111*, 18033–18038.
5. Xing, S.; Hu, C.; Qu, J.; He, H.; Yang, M. Characterization and reactivity of MnO_x supported on mesoporous zirconia for herbicide 2,4-D mineralization with ozone. *Environ. Sci. Technol*. **2008**, *42*, 3363–3368.
6. Tang, X.; Chen, J.; Huang, X.; Xu, Y.; Shen, W. Pt/MnO_x—CeO_2 catalysts for the complete oxidation of formaldehyde at ambient temperature. *Appl. Catal. B* **2008**, *81*, 115–121.
7. Nishimura, N.; Tanikawa, J.; Fujii, M.; Kawahara, T.; Ino, J.; Akita, T.; Fujino, T.; Tada, H. A green process for coupling manganese oxides with titanium(IV) dioxide. *Chem. Commun*. **2008**, 3564–3566.
8. Tada, H. *Encyclopedia of Surface and Colloid Science*; Hubbard, A.T., Ed.; Marcel Dekker: New York, NY, USA, 2002.
9. Zhang, H.; Chen, G.; Bahnemann, D.W. Photoelectrocatalytic materials for environmental applications. *J. Mater. Chem*. **2009**, *19*, 5089–5121.
10. Liu, G.; Wang, L.; Yang, H.G.; Cheng, H.-M.; Lu, G.Q. Titania-based photocatalysts-crystal growth, doping and heterostructuring. *J. Mater. Chem*. **2010**, *20*, 831–843.
11. Tada, H.; Jin, Q.; Nishijima, H.; Yamamoto, H.; Fujishima, M.; Okuoka, S.-I.; Hattori, T.; Sumida, Y.; Kobayashi, H. Titanium(IV) dioxide surface-modified with iron oxide as a visible light photocatalyst. *Angew. Chem. Int. Ed*. **2011**, *50*, 3501–3505.
12. Jin, Q.; Fujishima, M.; Tada, H. Visible-light-active iron oxide-modified anatase titanium(IV) dioxide. *J. Phys. Chem. C* **2011**, *115*, 6478–6483.
13. Muramatsu, Y.; Jin, Q.; Fujishima, M.; Tada, H. Visible-light-activation of TiO_2 nanotube array by the molecular iron oxide surface modification. *Appl. Catal. B* **2012**, *119–120*, 74–80.
14. Jin, Q.; Ikeda, T.; Fujishima, M.; Tada, H. Nickel(II) oxide surface-modified titanium(IV) dioxide as a visible-light-active photocatalyst. *Chem. Commun*. **2011**, *47*, 8814–8816.
15. Nolan, M. Surface modification of TiO_2 with metal oxide nanoclusters: A route to composite photocatalytic materials. *Chem. Commun*. **2011**, *47*, 8617–8619.

16. Nolan, M.; Iwaszuk, A.; Tada, H. Molecular metal oxide cluster-surface modified titanium(IV) dioxide photocatalysts. *Aust. J. Chem*. **2012**, *65*, 624–632.
17. Jin, Q.; Fujishima, M.; Nolan, M.; Iwaszukb, A.; Tada, H. Photocatalytic activities of tin(IV) oxide surface-modified titanium(IV) dioxide show a strong sensitivity to the TiO_2 crystal form. *J. Phys. Chem. C* **2012**, *116*, 12621–12626.
18. Papadimitriou, V.C.; Stefanopoulos, V.G.; Romanias, M.N.; Papagiannakopoulos, P.; Sambani, K.; Tudose, V.; Kiriakidis, G. Determination of photo-catalytic activity of un-doped and Mn-doped TiO_2 anatase powders on acetaldehyde under UV and visible light. *Thin Solid Films* **2011**, *520*, 1195–1201.
19. Fujishima, M.; Jin, Q.; Yamamoto, H.; Tada, H.; Nolan, M. Tin oxide-surface modified anatase titanium(IV) dioxide with enhanced UV-light photocatalytic activity. *Phys. Chem. Chem. Phys*. **2012**, *14*, 705–711.
20. Tan, B.J.; Klabunde, K.J.; Sherwood, P.M.A. XPS studies of solvated metal atom dispersed catalysts. Evidence for layered cobalt-manganese particles on alumina and silica. *J. Am. Chem. Soc*. **1991**, *113*, 855–861.
21. Tada, H.; Jin, Q.; Kobayashi, H. Prediction of the main route in the TiO_2-photocatalyzed degradation of organics in water by density functional theory calculations. *ChemPhysChem* **2012**, *13*, 3457–3461.